

Effect of surface porosity of catalytic supports on plasma-assisted catalysis for ammonia synthesis

S. Jaiswal,^{1, 2, a)} Zhe Chen,^{1, b)} Sankaran Sundaresan,¹ Bruce E Koel,¹ and Ahmed Diallo³

¹⁾Princeton University, Department of Chemical and Biological Engineering, Princeton, NJ 08544

²⁾Eastern Michigan University, Department of Physics and Astronomy, 240 Strong Hall, Ypsilanti, MI 48197

³⁾Princeton Plasma Physics Laboratory, 100 Stellarator Rd, Princeton, NJ 08540

A fundamental understanding of plasma-catalyst interactions is important for understanding reaction mechanisms, optimizing the catalyst, and increasing the efficiency of plasma-assisted catalytic process for ammonia (NH₃) synthesis. We report on the effect of the surface porosity of the catalyst support on this reaction carried out in a coaxial dielectric barrier discharge (DBD) plasma reactor. The discharge was created using a variable AC applied voltage at room temperature and near atmospheric pressure (550 Torr). Two catalyst supports were compared: porous silica (SiO₂) ceramic beads and smooth, non-porous soda lime glass beads of almost equal diameter (~1.5 mm) were used. N₂ conversion and the NH₃ synthesis rate was increased with increasing voltage for both supports, but the energy yield for NH₃ production increased for the SiO₂ beads and decreased for the glass beads. All three of these parameters were always higher when using the SiO₂ beads, which suggests that porosity can be a small advantage for plasma assisted NH₃ synthesis. Discharge and plasma properties were estimated from Lissajous plots and using calculations with the BOLSIG+ software. The effect of different catalyst supports on the physical properties of the discharge was negligible. High resolution optical emission spectra (OES) were used to explore the evolution of gas phase active species, N₂⁺, atomic N, electronically excited N₂, and atomic H (H_α, H_β), in the plasma in the presence of both supports. The relative concentration of these species was lower in the case of the porous SiO₂ beads for all applied voltages, which suggests that surface reactions are more significant than gas phase reactions for the formation of NH₃ in plasma assisted NH₃ synthesis.

I. INTRODUCTION

The Haber–Bosch (H–B) process is used industrially to produce NH₃ from N₂ and H₂ in a thermal catalytic process at high temperature (600–800 K) and high pressure (100–200 atm).¹ This process is energy intensive and consumes almost 2% of the world’s annual energy supply.² Possible alternative processes to produce NH₃ under milder reaction conditions, such as one utilizing a non-thermal plasma (NTP), are being investigated extensively.^{3,4} Non-thermal, cold, or non-equilibrium plasmas can produce high energy electrons and create excited molecular species and radicals in the gas phase at ambient conditions of lower temperatures and pressures, enabling reactions with high energy barriers to occur.^{5,6} This also enables small scale, fast on/off operations, and possibly reduced energy costs.² Therefore, NTP-assisted catalysis for NH₃ synthesis has recently gained increasing attention.^{1,5,7–9}

Investigations using various NTP reactors, including experiments and kinetic modeling, have been performed to understand the fundamentals of plasma-assisted NH₃ synthesis and control mechanisms.^{1,5,10–14} Dielectric barrier discharges (DBDs) in different configurations (planar and coaxial)^{11–14} are popular NTP reactors and experiments have been performed with different metal electrodes¹ and dielectric¹² and ferroelectric materials.^{13,14} Combining NTPs with heterogeneous catalysts improves the performance for many reactions, including NH₃ synthesis, dry reforming of CH₄, and many

more.^{7,15–17} A synergy between the plasma and catalysts is often invoked to explain the enhancement in reaction rate or selectivity, which e.g., enables NH₃ synthesis to proceed at low temperature and pressure conditions.² Finding better catalysts and catalyst supports that are optimal in the presence of plasma has been an emerging area of research in recent years. The behavior of plasma in presence of a packed bed of catalysts is also an ongoing area of research.⁵

Previous investigations showed that changing the physical properties of the catalyst material such as dielectric constant, surface area, particle size, and void fraction can alter the plasma properties as a result of the modified electric field.^{18–22} In addition, the exposures of the plasma to a catalyst can change the chemical or electronic properties of the catalyst, modify surface reaction pathways, change the catalyst morphology, or improving catalyst dispersion.^{18,21,23,24} Any or all of these changes may improve the catalyst performance, which is usually quantified as overall reaction conversion and reaction rate.

Specifically for plasma-assisted catalysis for NH₃ synthesis, a wide variety of catalysts and catalyst supports have been evaluated.^{13,18,22–25} Patil *et al.*¹⁸ investigated the effect of a range of bare catalyst supports including α -Al₂O₃, γ -Al₂O₃, MgO, CaO, TiO₂, and quartz wool on the synthesis of NH₃ in a DBD reactor. Mehta *et al.*¹ investigated the plasma-assisted catalytic synthesis of NH₃ using a range of γ -Al₂O₃ supported metal catalysts (Fe, Ru, Co, Ni, and Pt), as well as the bare γ -Al₂O₃ support particles, in a DBD reactor. They concluded that a key elementary step, the dissociative adsorption of N₂ on metallic catalyst surfaces, can be facilitated by the vibrational excitation of N₂ by energetic electrons in the plasma.¹ The simulation study by Hong *et al.*¹⁰ showed that adsorbed

^{a)}Electronic mail: surabhijaiswal73@gmail.com

^{b)}Co-first author and contribute to equally to this study

hydrogen H(s) on Fe is essential for plasma-assisted catalytic NH_3 synthesis.

In recent years, increasing effort has also been made to understand the plasma behavior, e.g. plasma generation and propagation, in the packed bed reactors that are typically used, where there can be a wide variety of catalysts and support materials with different shapes, sizes, and pore dimensions. As shown in a two-dimensional simulation of an atmospheric pressure DBD plasma in He, plasma can be generated inside catalyst pores.²² In later work, Zhang *et al.*²⁶ modeled the plasma generation in a pore on a dielectric surface. They observed that ionization, electric fields, and electron densities can be larger inside the pores compared to the bulk, and the applied voltage, pore dimensions, and particle shape are critical parameters. Materials of low dielectric constant can have microdischarges in smaller pores, indicating that common catalyst supports such as $\gamma\text{-Al}_2\text{O}_3$ and SiO_2 , which have low dielectric constants, should have microdischarges in their pores despite the small pore sizes.²² In another investigation, it was found that at higher voltages, ionization can take place mainly inside the pores.²⁷ From these investigations, it is clear that the surface porosity of the catalyst support can be an important factor in plasma-assisted catalysis of NH_3 synthesis, and thus it is important to conduct additional studies of the effect of surface porosity in order to advance our fundamental understanding of this reaction process.

Recently, a limited number of experiments have been performed by combining optical and electrical diagnostics of the plasma to better characterize the plasma, understand the role of different catalysts, and develop reactions mechanisms based on these measurements.^{13,14,25,28} For example, Wang *et al.*²⁸ performed experiments with Ni, Cu, and Fe catalysts supported on $\gamma\text{-Al}_2\text{O}_3$ in which they performed various diagnostics for plasma characterization and surface analysis of the materials. However, there has not yet been a report of a study that explored the effect of surface porosity on the overall reaction rate, as well as the plasma characteristics, for plasma-assisted catalysis of NH_3 synthesis.

In this paper, we report our results that combine the use of electrical and optical diagnostics of the plasma to measure the discharge characteristics and probe several active gas phase species present in the plasma in a packed-bed coaxial DBD reactor using either porous SiO_2 beads or nonporous soda lime glass (referred to as “glass”) beads and at the same time measured experimentally the N_2 conversion and NH_3 production using gas chromatography (GC).

II. EXPERIMENTAL SETUP

Fig. 1(a) shows a schematic diagram of the experimental setup. The coaxial DBD reactor consisted of a quartz tube (0.4 in. I.D., 0.5 in. O.D.), a 2.25-in. long copper woven wire mesh wrapped around the outside of the quartz tube that served as the grounded electrode, and a 0.125-in. diameter stainless steel rod covered by a 0.25-in. O.D. quartz tube, which served as the high voltage (HV) electrode, running down the center of the larger quartz tube. An AC power

source (Information Unlimited, PVM500) with a frequency of 20 kHz was used to produce the DBD plasma.

A. Reaction kinetics experiments

Two different types of dielectric spherical beads, which had the same diameter (~ 1.5 mm) but had different surface porosities were used in these experiments: (i) porous SiO_2 (surface area of $300 \text{ m}^2/\text{g}$) beads, and (ii) non-porous soda lime glass beads. Prior to experiments, the porous SiO_2 beads were dried in-situ at 523 K for 2 h under 50 mL/min N_2 . The glass beads were dried in-situ at 423 K for 2 h under 50 mL/min N_2 . All experiments were run at room temperature, with the reactor pressure set to 550 Torr, and no external reactor heating used. The flow rates of N_2 (Airgas, 99.999%) and H_2 (Praxair, 99.99%) into the reactor were controlled by mass flow controllers (Teledyne Hastings Instruments, 300 Series). The total flow rate was kept at 26.5 mL/min. The NH_3 produced in the reactor was quantified by using an online gas chromatograph (Agilent, 7890A) with a CP-Volamine column (Agilent, CP-7447) and a thermal conductivity detector.

B. Plasma characterization

Signals of applied voltage, current, and the voltage across an external capacitor (1000 pF) connected in series with the reactor were recorded by an oscilloscope (GW Instek, GDS-1054B). A Lissajous plot, which is a plot of charge vs. applied voltage, was constructed from the signals of the capacitor voltage and applied voltage.²⁹ Discharge power was estimated from the Lissajous plot as the product of frequency and the area enclosed by the plot.²⁹ We then used BOLSIG+³⁰ to estimate the mean electron temperature of the plasma using the reduced electric field as an input, which was estimated from the Lissajous plot following Butterworth *et al.*³¹ and Mei *et al.*³² We also estimated the electron number density from the Lissajous plot using a simple technique described by Hong *et al.*³³, in which the electron mobility was obtained by using BOLSIG+.³⁰ Optical emission spectra were recorded using a high resolution (≤ 0.05 nm) spectrometer (Princeton Instruments SpectraPro[®] HRS-500). The optical arrangement consisted of a multiwavelength (200–1000 nm) collimator (Fig. 1(b)) that is connected to the spectrometer via a 1-m long optical fiber. The optical setup was located at a distance of ~ 10 cm from the reactor. A broad spectrum was measured by using a 1200 g/mm grating in the Step and Glue mode that enabled covering a wavelength range from 300 - 1100 nm without compromising the resolution. The spectrometer integration time was set to between 1 - 15 s to compensate for the varying signal from the plasma.

Measured signals of both applied voltage and current for the reactor packed with glass beads at 11 and 16 kV are shown in Fig. 2(a). Both the number and the intensity of microdischarges increased with applied voltage. Lissajous plots obtained using a packed bed of glass beads for applied voltage 11 and 16 kV are shown by Fig. 2(b). As the applied volt-

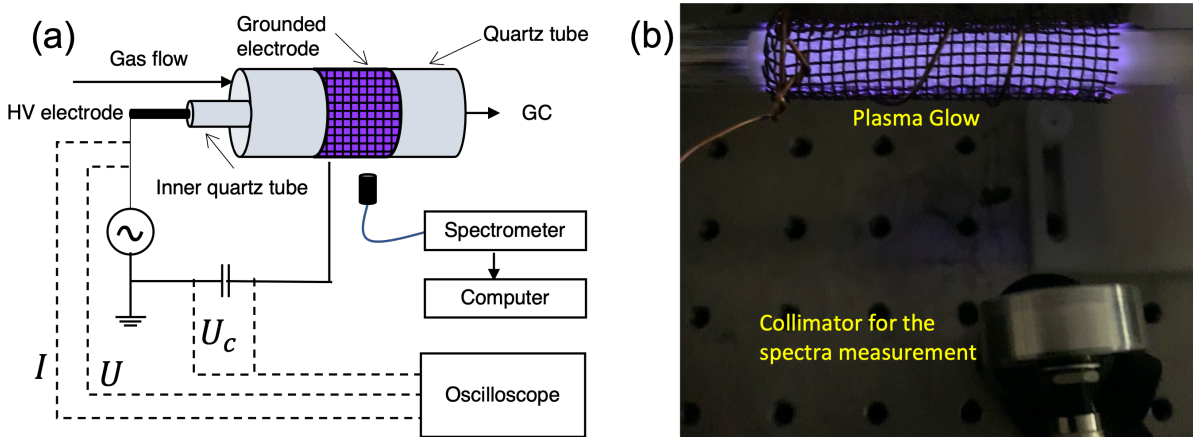


FIG. 1: (a) Schematic diagram of the experimental setup. Solid lines and dashed lines represent electrical circuits and electrical signals, respectively. (b) Photograph of the plasma glow in the DBD reactor packed with glass beads and the arrangement of the optical collimator for the OES measurements.

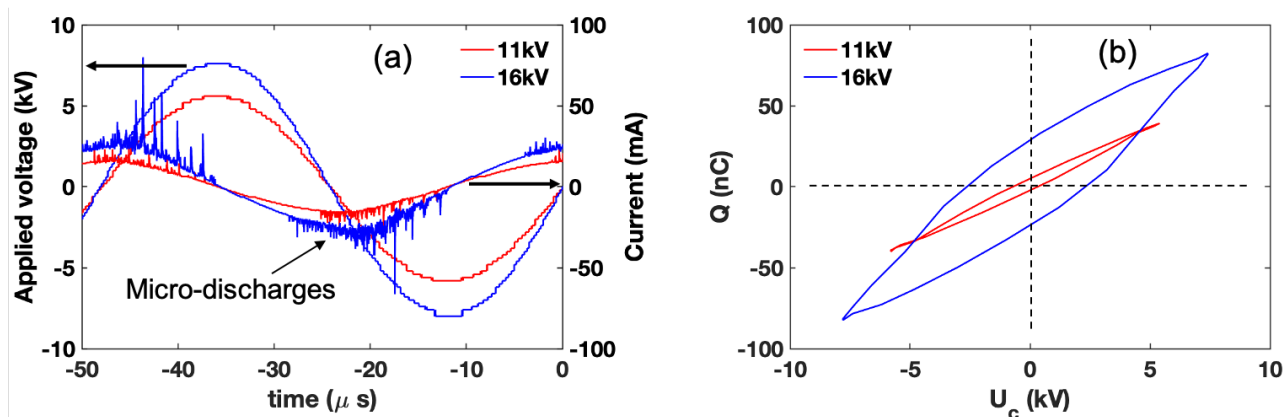


FIG. 2: (a) Applied voltage and current signals and (b) the corresponding Lissajous plots for the DBD reactor packed with glass beads at an applied voltage of 11 and 16 kV. Conditions: 550 Torr, 26.5 mL/min, $N_2:H_2=1:3$.

age was increased, the area enclosed by the plot increased, indicating that the consumed power increased. Similarly, the reduced electric field increased with applied voltage, and the values of the reduced electric field at various applied voltages are shown in Table S1 of the Supplementary Information (SI).

III. RESULTS AND DISCUSSION

A. Materials characterization

Surface area and pore size distribution of the SiO_2 beads was measured using a Brunauer–Emmett–Teller (BET) analyzer (Micromeritics 3Flex). The SiO_2 surface area was $300 \text{ m}^2/\text{g}$ and the average pore size was 8 nm. The glass beads were nonporous with a calculated geometric surface area of $3.4 \times 10^{-3} \text{ m}^2/\text{g}$ assuming 2.1 as the surface roughness.¹⁰ SEM images were taken for both the SiO_2 and glass beads for additional characterization, and these are shown in Fig. 3. For better visualization, a zoomed-in view of each of the re-

spective images in Figs. 3 (a) and (c) (marked by yellow rectangles) are shown in Figs. 3 (b) and (d). The surfaces of the nanoporous SiO_2 beads also have a microscale roughness much larger than that of the nonporous glass beads.

B. Effects of surface porosity and applied voltage

Experiments were conducted using a feed ratio of $N_2:H_2 = 1:3$ at various applied voltages for the discharge. N_2 conversion was calculated from the NH_3 mole fraction measured by the GC under each experimental condition. As shown in Fig. 4, N_2 conversion increased with increased applied voltage for both SiO_2 and glass beads, with the SiO_2 beads producing higher N_2 conversion compared to the glass beads. Electron number densities were estimated from the Lissajous plots measured for each experiment. Fig. 5 shows that a higher applied voltage resulted in a higher electron number density, although this effect is much less for packing with porous SiO_2 beads. Surface porosity of the packing beads clearly has an in-

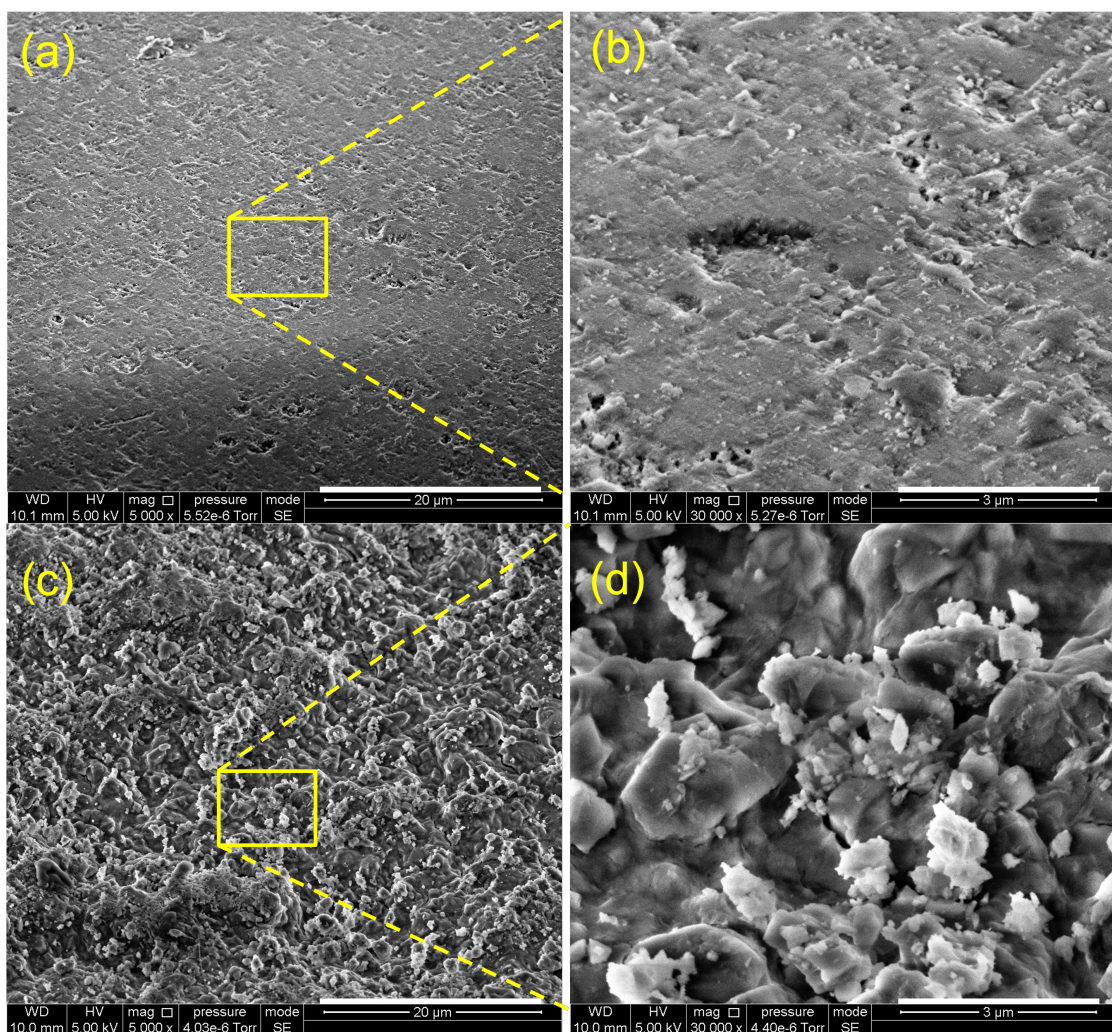


FIG. 3: SEM images of the surface of a nonporous glass bead (a and b) and a porous SiO₂ bead (c and d). Scale bars are 20 μm for (a) and (c) and 3 μm for (b) and (d).

fluence on the electron number density, such that at the same applied voltage, the electron number density was higher when using the porous SiO₂ beads than with the nonporous glass beads, however, the difference in the electron densities is of little significance at the higher applied voltages.

It was reported that the N₂:H₂ feed ratio had an effect on the observed rate of NH₃ production.^{1,13} For example, when using γ-Al₂O₃ and Ru/γ-Al₂O₃ catalysts in the reactor, the optimal ratio of N₂:H₂ was found to lie between 1:1 and 3:1, richer in N₂ compared to the stoichiometric ratio.¹ Thus, it is important to also compare the reaction rates and energy yields in the presence of SiO₂ and glass beads at their respective N₂:H₂ optimal feed ratios. We first performed NH₃ synthesis experiments with both catalyst support packing materials using various feed ratios to determine the N₂:H₂ ratio that gave the highest reaction rate. As shown in Fig. 6, with SiO₂ beads, the optimal feed ratio was 1:2. This indicates that a nitrogen-rich feed resulted in a higher observed NH₃ production rate. However, further increases in the N₂:H₂ ratio reduced the reaction rate. With glass beads, the optimal N₂:H₂ ratio was

1:3, which represents a less nitrogen-rich feed from that using SiO₂ beads.

Next, we compared the NH₃ energy yields for the DBD reactor packed with SiO₂ and glass beads, as well as the observed NH₃ production rates of these two catalyst support materials at their respective optimal feed ratios (N₂:H₂=1:2 for SiO₂ and 1:3 for glass beads). As shown in Fig. 7, packing with SiO₂ beads gave a higher NH₃ energy yield than that when using glass beads except at the lowest applied voltage tested at 13 kV. A higher observed NH₃ production rate was also seen for packing with SiO₂ beads compared to that when using glass beads at all of the voltages tested in our experiments. With increased applied voltage, the NH₃ energy yield increased when using SiO₂ beads, but decreased for glass beads, and the observed NH₃ production rate increased more significantly in the presence of SiO₂ beads compared to glass beads. This may be explained by the generation of more surface microdischarges at higher voltages due to the porous surface structure of SiO₂ compared to that of the glass beads.

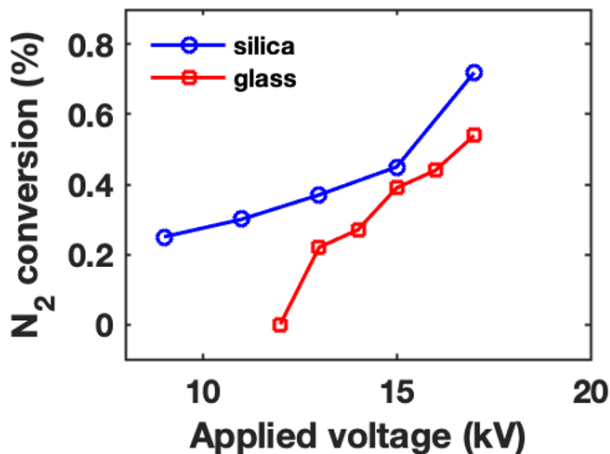


FIG. 4: Observed N₂ conversion for different applied voltages for the DBD reactor packed with SiO₂ or glass beads. Reaction conditions: 550 Torr, 26.5 mL/min, N₂:H₂=1:3.

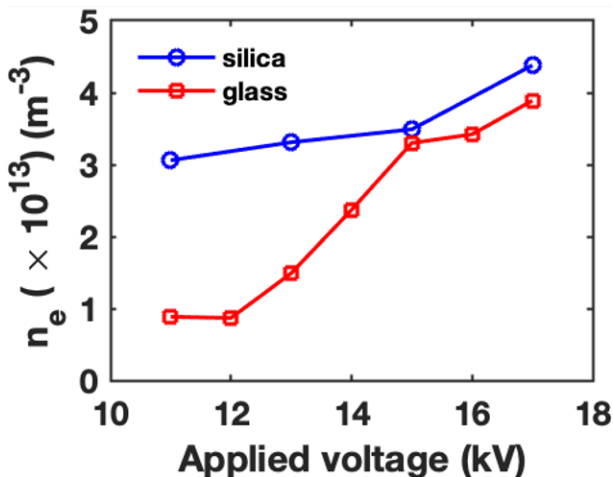


FIG. 5: Electron number density determined from Lissajous plots for different applied voltages for the DBD reactor packed with SiO₂ or glass beads. Reaction conditions: 550 Torr, 26.5 mL/min, N₂:H₂=1:3.

C. OES spectra and intensities of gas phase species

OES spectra of the plasma were measured during operation of the DBD reactor packed with SiO₂ or glass beads at several applied voltages. Fig. 8 shows a representative OES spectrum from the DBD reactor packed with glass beads with an applied voltage of 16 kV as an example. Observation of the N₂ second positive system and the N₂ first positive system suggests that N₂ molecules are electronically excited by electrons in the plasma: $e + \text{N}_2 \longrightarrow e + \text{N}_2^*$. Observation of the N₂⁺ first negative system at 391.2 nm and 427 nm confirmed electron-impact ionization in the plasma: $e + \text{N}_2 \longrightarrow 2e + \text{N}_2^+$. The hydrogen Balmer lines, with H_β at 486.2 nm and H_α at 656 nm, indicates that atomic H was present in the plasma. The existence of atomic N species in the plasma was confirmed by

emission lines at several wavelengths: 742, 818.5, 822, 824, 939, and 1011 nm. Identification of H Balmer atomic lines and atomic N suggests the dissociation of N₂ and H₂.²⁸ We did not clearly observe an NH line at 336 nm, but this might overlap with the 337-nm line of the N₂ second positive system. The OES spectra provide direct evidence of the existence of several gas phase active species in the N₂-H₂ plasma during NH₃ synthesis such as electronically excited molecular nitrogen N₂^{*}, N₂⁺, N, and H. The spectrum shown here is mostly consistent with previous reports^{13,28} on N₂-H₂ plasma generated in a DBD reactor with different packing materials. However, those other reported spectra were not well resolved and so the measurement of an NH line at 336 nm was obtained by using the shoulder of the N₂ second positive system at 337 nm. We did not detect any peak at 336 nm even at very high resolution (0.05 nm) measured using a 2400 g/mm grating, and therefore, we do not assign an NH line in our spectra. The normalized intensities of emission lines for N₂⁺, H_α, H_β, and N (939 nm) (relative to the intensity of the N₂ line at 357 nm¹³) for the plasma during operation of the DBD reactor packed with SiO₂ and glass beads are shown in Figs. 9(a)-(d) for several applied voltages. For both packing materials, the relative intensities of all of the emission lines decreased with increasing applied voltage. Assuming that the ratio between band intensities is equivalent to that between the concentrations¹³ of the emitting species, we can see that increasing applied voltage increased the plasma energy that was expended in electronically exciting N₂ molecules more than in generating N₂⁺, H, and N through electron-impact ionization and electron-impact dissociation. Furthermore, as shown in Fig. 9, relative intensities of N₂⁺, H_α, and atomic nitrogen lines were found to be higher with glass bead packing than with SiO₂. This is because at the same applied voltage, the plasma had a lower reduced electric field and hence a lower mean electron temperature for SiO₂ relative to glass packing. The values for the reduced electric field and mean electron energy for these experiments are provided in the SI. Because the rate constants for electron-impact ionization ($e + \text{N}_2 \longrightarrow 2e + \text{N}_2^+$) and electron-impact dissociation ($e + \text{N}_2 \longrightarrow e + 2\text{N}$ and $e + \text{H}_2 \longrightarrow e + 2\text{H}$) increase with mean electron temperature³⁴, these reactions proceed at lower reaction rates in the presence of SiO₂ compared to glass beads and lead to fewer N₂⁺, H, and N species in the plasma.

We also compared the normalized intensities of N₂⁺, H_β, H_α, and N lines at 742 nm and 939 nm for the DBD reactor packed with SiO₂ and glass beads at the same plasma power of 11 W, corresponding to an applied voltage of 17 kV for SiO₂ and 16 kV for glass beads. Fig. 10 shows the normalized relative intensities of these lines, where the intensities were ratioed against the N(357 nm) line and then normalized with respect to those intensities for glass (set to unity) following the same approach as that by Wang *et al.*²⁸ The NH₃ yield is also shown on the right of Fig. 10, which was normalized with respect to the yield obtained with glass bead packing (set to unity). At the same plasma power, the intensities of the five emission lines monitored were found to be lower in the presence of SiO₂ than glass beads. As noted before, this could be due to a lower mean electron energy with SiO₂ packing

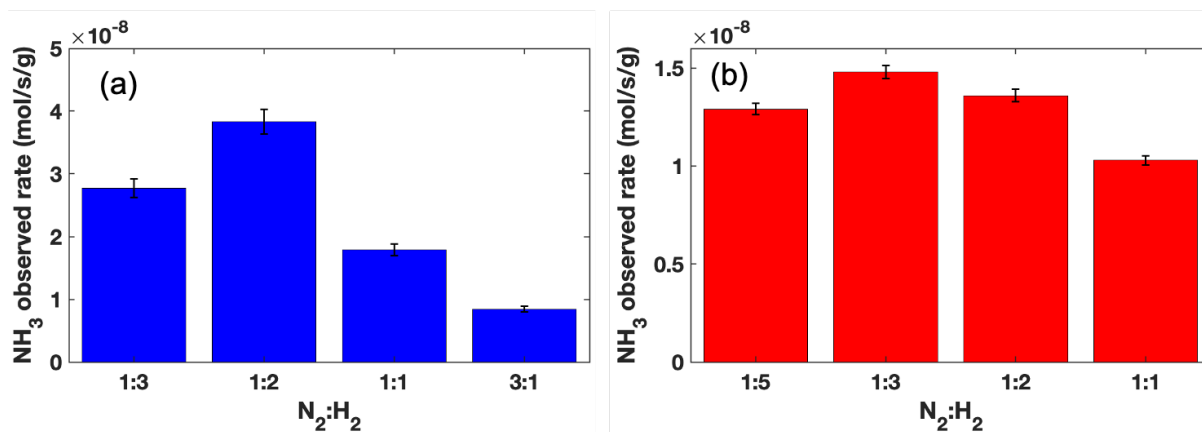


FIG. 6: NH_3 observed production rate at different $\text{N}_2:\text{H}_2$ feed ratios for the DBD reactor packed with (a) SiO_2 and (b) glass beads. Reaction conditions: 550 Torr, 26.5 mL/min, 17 kV.

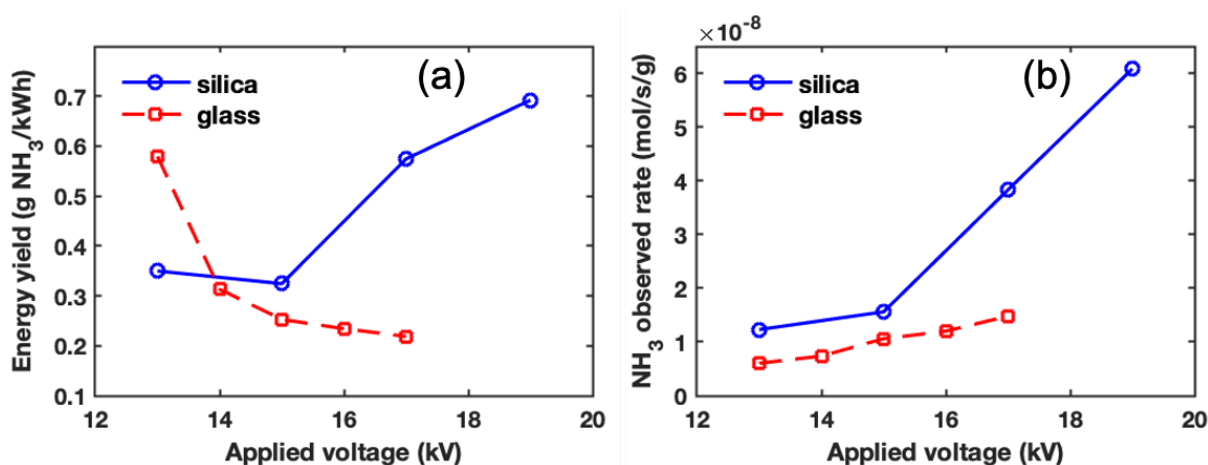


FIG. 7: (a) NH_3 energy yield and (b) NH_3 observed production rate at optimal $\text{N}_2:\text{H}_2$ ratio (1:2 for SiO_2 and 1:3 for glass beads) for different applied voltages. Reaction conditions: 550 Torr, 26.5 mL/min.

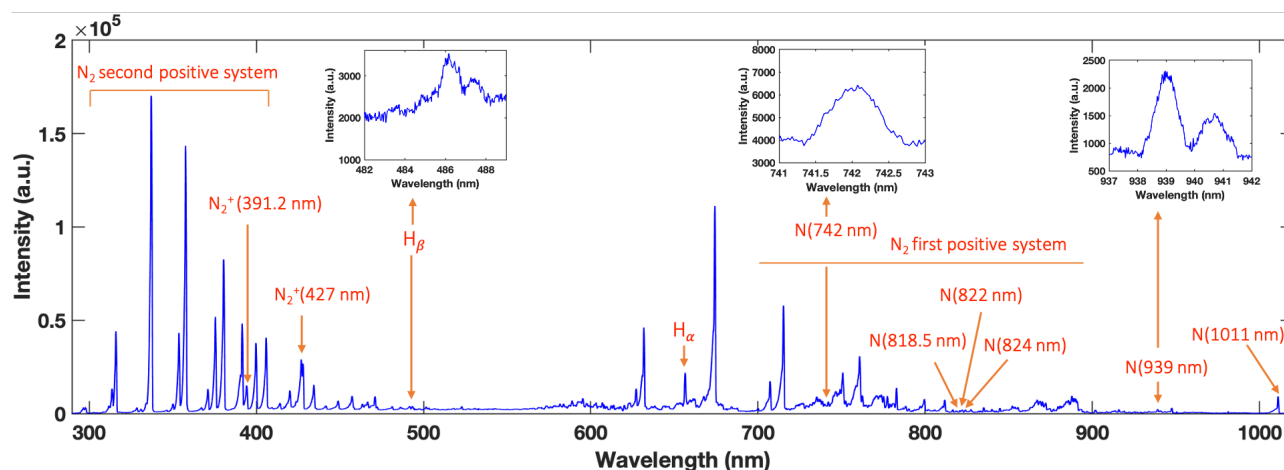


FIG. 8: OES spectrum of the plasma during operation of the DBD reactor packed with glass beads at an applied voltage of 16 kV. Conditions: 550 Torr, 26.5 mL/min, $\text{N}_2:\text{H}_2=1:3$.

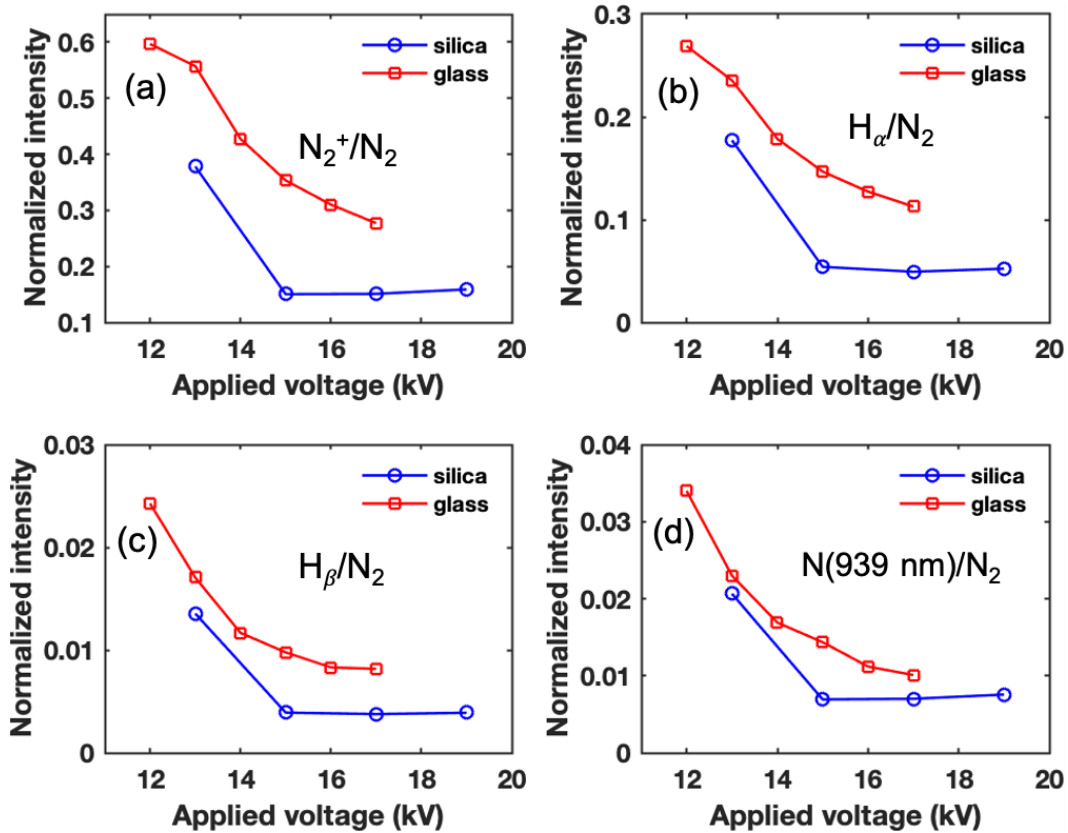
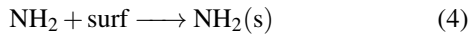
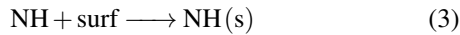
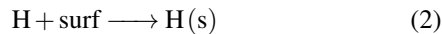
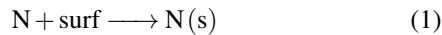


FIG. 9: Normalized intensities of N_2^+ , H_α , H_β , and N (939 nm) emission lines from the plasma during operation of the DBD reactor packed with SiO_2 or glass beads. Conditions: 550 Torr, 26.5 mL/min, $N_2:H_2=1:3$.

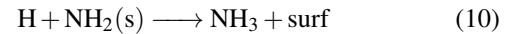
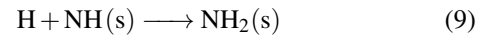
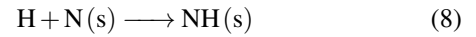
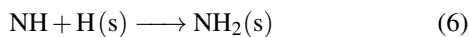
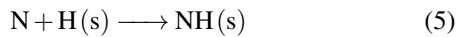
leads to lower concentrations of the related gas phase species. Interestingly, the observed NH_3 yield with SiO_2 packing was found to be more than 1.5 times higher than that with glass packing even though SiO_2 packing had lower concentrations of active plasma species such as N_2^+ , H, and N.

As concluded by Hong *et al.*¹⁰ in their zero-dimensional kinetic modelling results, radical adsorption and Eley–Rideal (E–R) surface reactions can occur on non-metallic surfaces such as Al_2O_3 , as given below.

Radical adsorption:



E–R reactions:



The rate constants for these surface reactions can be calculated using the following equation¹⁰:

$$k = \left[\frac{\Lambda}{D} + \frac{V}{A} \frac{2(2-\gamma)}{\bar{v}\gamma} \right]^{-1} S_T^{-1} \quad (11)$$

where Λ is the diffusion length, D is the diffusion coefficient, V is the discharge volume, A is the surface area, γ is the sticking coefficient, \bar{v} is the thermal velocity, and S_T is the total surface site density. As shown by Eq. (11), rate constants for radical adsorption and E–R reactions increase with increasing surface area. As a result, SiO_2 beads have higher surface area available for radical adsorption and E–R reactions compared to nonporous glass beads, which results in higher rate constants for these surface reactions.

Although the OES data show that concentrations of N and H were lower in the presence of SiO_2 beads than glass

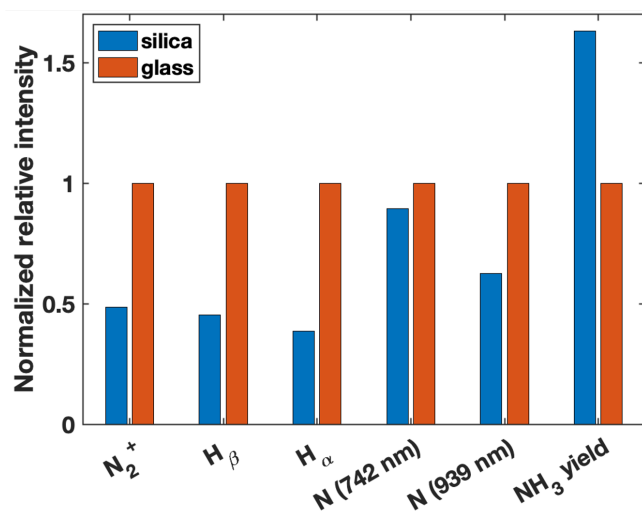


FIG. 10: Normalized relative intensities of N_2^+ , H_β , H_α , N(742 nm), and N(939 nm) emission lines from the plasma during operation of the DBD reactor packed with SiO_2 and glass beads at 11 W. Conditions: 550 Torr, 26.5 mL/min, $N_2:H_2=1:3$, and an applied voltage of 17 kV for SiO_2 and 16 kV for glass beads.

beads, a higher NH_3 observed reaction rate and a higher NH_3 yield were obtained with SiO_2 packing, suggesting that these species must be consumed more in the SiO_2 bed. This is likely due to the fact that the higher surface porosity of SiO_2 provided larger surface area, which resulted in higher rate constants for surface reactions in Eqns. (1–10). The simulation study by Hong *et al.* showed that radical adsorption and E–R reactions can proceed on non-metallic surfaces and provide a pathway to NH_3 even in the absence of catalytic metal nanoparticles.¹⁰ Thus, our operando studies combining OES and GC data together indicate that surface porosity had important effects on the overall reaction and surface chemistry had a more significant contribution to the production of NH_3 than gas phase chemistry in these porosity studies.

IV. CONCLUSION

We have investigated the effect of surface porosity of catalytic supports on the reaction rate and energy yield of plasma-assisted catalysis for NH_3 synthesis. We performed NH_3 synthesis experiments using a coaxial DBD reactor packed with two different catalyst support materials, i.e., nanoporous SiO_2 beads and non-porous soda lime glass beads, at several applied voltages (10–20 kV) at near atmospheric pressure (550 Torr). Measurements of NH_3 concentrations at the reactor outlet using a GC found that both the observed NH_3 production rates and NH_3 energy yields were enhanced in the presence of porous SiO_2 beads compared to nonporous glass beads at the respective optimal $N_2:H_2$ feed ratios for the two catalyst support materials.

In conjunction with the NH_3 synthesis measurements, we made operando measurements of Lissajous plots to charac-

terize the plasma by the reduced electric field and electron number density, and measurements of high resolution OES spectra to obtain the relative concentrations of several active species N_2^+ , N, and H, in the plasma. OES measurements showed that the concentrations of N_2^+ , N, and H were lower for plasma in the presence of SiO_2 than glass beads. Despite lower concentrations of N_2^+ , N, and H in the gas phase, the DBD reactor packed with SiO_2 beads provided a higher NH_3 yield than when packed with glass beads. This suggests that the active species in the gas phase were consumed more in the bed of SiO_2 beads than glass beads, which is likely due to the fact that SiO_2 provided larger surface area than glass. This shows that surface porosity of the catalyst support material has a significant effect on the plasma properties, reaction mechanism, and NH_3 yield, and that surface reaction pathway contributes most significantly to the overall reaction of plasma-assisted NH_3 synthesis. Higher surface porosity provides more surface sites for radical adsorption and the subsequent E–R reactions, resulting in higher overall reaction rate of plasma-assisted NH_3 synthesis.

ACKNOWLEDGEMENTS

The research described in this paper was, in part, supported by the Laboratory Directed Research and Development (LDRD) Program at Princeton Plasma Physics Laboratory, a national laboratory operated by Princeton University for the U.S. Department of Energy under Prime Contract No. DE-AC02-09CH11466. The United States Government retains a non-exclusive, paid-up, irrevocable, world-wide license to publish or reproduce the published form of this manuscript, or allow others to do so, for United States Government purposes. BEK acknowledges partial support of this work by the U.S. Department of Energy, Office of Science, Office of Fusion Energy Sciences under award number DE-SC0020233. ZC acknowledges partial support by the Program in Plasma Science and Technology (PPST) at Princeton University. SJ acknowledges Dr. Arthur Dogariu for providing the high resolution spectrometer and Dr. Evan Aguirre for helping with spectral analysis and reviewing the manuscript. The authors acknowledge Sonia Arumuganainar for the BET measurements. The authors acknowledge the use of Princeton’s Imaging and Analysis Center (IAC), which is partially supported by the Princeton Center for Complex Materials (PCCM), a National Science Foundation (NSF) Materials Research Science and Engineering Center (MRSEC; DMR-2011750).

DATA AVAILABILITY

The data that support the findings of this study are available from the corresponding author upon reasonable request.

¹P. Mehta, P. Barboun, F. A. Herrera, J. Kim, P. Rumbach, D. B. Go, J. C. Hicks, and W. F. Schneider, *Nature Catalysis* **1**, 269–275 (2018).

²A. Bogaerts and E. C. Neyts, *ACS Energy Lett.* **3**, 1013–1027 (2018).

³A. Bogaerts, X. Tu, J. C. Whitehead, G. Centi, L. Lefferts, O. Guaitella, F. Azzolina-Jury, H.-H. Kim, A. B. Murphy, W. F. Schneider, T. Nozaki,

- J. C. Hicks, A. Rousseau, F. Thevenet, A. Khacef, , and M. Carreon, *J. Phys. D: Appl. Phys.* **53**, 443001 (2020).
- ⁴J. G. Chen, R. M. Crooks, L. C. Seefeldt, K. L. Bren, and R. M. B. et al, *Science* **360** (6391) (2018), 10.1126/science.aar6611.
- ⁵A. B. et al, *J. Phys. D: Appl. Phys.* **53**, 443001 (2020).
- ⁶J. Hong, S. Prawer, and A. B. Murphy, *ACS Sustainable Chem. Eng.* **6**, 15–31 (2018).
- ⁷K. Sugiyama, K. Akazawa, M. Oshima, H. Miura, T. Matsuda, and O. Nomura, *Plasma Chem. Plasma Process.* **6**, 179–193 (1986).
- ⁸T. Mizushima, K. Matsumoto, H. Ohkita, and N. Kakuta, *Plasma Chem. Plasma Process.* **27**, 1–11 (2007).
- ⁹G. Akay, , and K. Zhang, *Ind. Eng. Chem. Res.* **56**(2), 457–468 (2017).
- ¹⁰J. Hong, S. Pancheshnyi, E. Tam, J. J. Lowke, S. Prawer, and A. B. Murphy, *J. Phys. D: Appl. Phys.* **50**, 154005 (2017).
- ¹¹J. Hong, M. Aramesh, O. Shimoni, D. H. Seo, S. Yick, A. Greig, C. Charles, S. Prawer, and A. B. Murphy, *Plasma Chemistry and Plasma Processing* **50**, 917–940 (2016).
- ¹²X. Zhu, X. Hu, X. Wu, Y. Cai, H. Zhang, and X. Tu, *J. Phys. D: Appl. Phys.* **53**, 164002 (2020).
- ¹³A. Gómez-Ramírez, J. Cotrino, R. M. Lambert, , and A. R. González-Elipe, *Plasma Sources Sci. Technol.* **24**, 065011 (2015).
- ¹⁴A. Gómez-Ramírez, A. M. Montoro-Damas, J. Cotrino, R. M. Lambert, and A. R. González-Elipe, *Plasma Processes and Polymers* **14**, 1600081 (2017).
- ¹⁵E. C. Neyts, K. K. Ostrikov, M. K. Sunkara, and A. Bogaerts, *Chem. Rev.* **115**, 13408–13446 (2015).
- ¹⁶L. Wang, Y. Yi, C. Wu, H. Guo, and X. Tu, *Angew. Chem., Int. Ed.* **56**, 13679–13683 (2017).
- ¹⁷L. Wang, Y. Y. Yi Yi, H. Guo, and X. Tu, *ACS Catal.* **8**, 90–100 (2018).
- ¹⁸B. S. Patil, *Plasma (Catalyst) Assisted Nitrogen Fixation: Reactor Development for Nitric Oxide and Ammonia Production*, Ph.D. thesis, Eindhoven University of Technology (2017).
- ¹⁹F. A. Herrera, , G. H. Brown, P. B. abd Nazli Turan, P. Mehta, W. F. Schneider, J. C. Hicks, and D. B. Go, *J. Phys. D: Appl. Phys.* **52**, 224002 (2019).
- ²⁰Z. ul Islam Mujahid, J. Kruszelnicki, A. Hala, and M. J. Kushner, *Chemical Engineering Journal* **382**, 123038 (2020).
- ²¹J. C. Whitehead, *Frontiers of Chemical Science and Engineering* **13**, 264–273 (2019).
- ²²Y.-R. Zhang, E. C. Neyts, and A. Bogaerts, *J. Phys. Chem. C* **120**, 25923–25934 (2016).
- ²³P. Barboun, P. Mehta, F. A. Herrera, D. B. Go, W. F. Schneider, and J. C. Hicks, *ACS Sustainable Chem. Eng.* **7** (9), 8621–8630 (2019).
- ²⁴P. Mehta, P. Barboun, D. B. Go, J. C. Hicks, , and W. F. Schneider, *ACS Energy Lett.* **4** (5), 1115–1133 (2019).
- ²⁵F. Gorky, M. A. Carreon, and M. L. Carreon, *IOP SciNotes* **1**, 024801 (2020).
- ²⁶Y.-R. Zhang, E. C. Neyts, and A. Bogaerts, *Plasma Sources Sci. Technol.* **27**, 055008 (2018).
- ²⁷J.-G. Gu, Y. Zhang, M.-X. Gao, H.-Y. Wang, Q.-Z. Zhang, L. Yi, and W. Jiang, *Journal of Applied Physics*, **125**, 153303 (2019).
- ²⁸Y. Wang, M. Craven, X. Yu, J. Ding, P. Bryant, J. Huang, and X. Tu, *ACS Catal.* **9**, 10780–10793 (2019).
- ²⁹H. E. Wagner, R. Brandenburg, K. V. Kozlov, A. Sonnenfeld, P. P. Michel, and J. F. Behnke, *Vacuum* **71** (3), 417–436 (2003).
- ³⁰G. J. M. Hagelaar and L. C. Pitchford, *Plasma Sources Science and Technology* **14** (4), 722 (2005).
- ³¹T. Butterworth, R. Elder, and R. Allen, *Chemical Engineering Journal* **293**, 55–67 (2016).
- ³²D. Mei, X. Zhu, Y. L. He, J. D. Yan, and X. Tu, *Plasma Sources Science and Technology* **24** (1), 015011 (2014).
- ³³J. Hong, M. Aramesh, O. Shimoni, D. H. Seo, S. Yick, A. Greig, C. Charles, S. Prawer, and A. B. Murphy, *Plasma Chemistry and Plasma Processing* **36**, 917–940 (2016).
- ³⁴E. Carrasco, M. Jiménez-Redondo, I. I. Tanarro, and V. J. Herrero, *Physical Chemistry Chemical Physics*, **13** (43), 19561–19572 (2011).